Journal of Molecular Structure 1058 (2014) 41–50

Contents lists available at ScienceDirect

Journal of Molecular Structure

journal homepage: www.elsevier.com/locate/molstruc

Molecular structure and vibrational analysis on (*E*)-1-(3-methyl-2,6-diphenyl piperidin-4-ylidene) semicarbazide

A. Dhandapani [a], S. Manivarman [a,*], S. Subashchandrabose [b], H. Saleem [c]

[a] PG and Research Dept. of Chemistry, Government Arts College, C-Mutlur, Chidambaram 608 102, Tamil Nadu, India
[b] Dept. of Physics, M. A. R. College of Engineering & Technology, Trichy 621 316, Tamil Nadu, India
[c] Dept. of Physics, Annamalai University, Annamalainagar 608 002, Tamil Nadu, India

HIGHLIGHTS

- Structural properties of EMDPS.
- TED.
- NBO.
- ICT Calculations.
- Band gap energy.

GRAPHICAL ABSTRACT

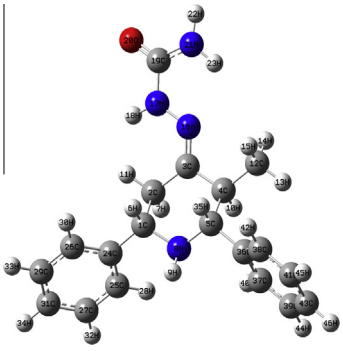

ARTICLE INFO

Article history:
Received 9 July 2013
Received in revised form 13 September 2013
Accepted 26 September 2013
Available online 15 October 2013

Keywords:
FT-IR
FT-Raman
TED
NBO
HOMO–LUMO
EMDPS

ABSTRACT

The (*E*)-1-(3-methyl-2,6-diphenylpiperidin-4-ylidene)semicarbazide (EMDPS) was synthesized and characterized by FT-IR, FT-Raman and on the basis of DFT calculation. To identify the stable structure the conformational analysis was performed using B3LYP/6-311++G(d,p) level of calculation. For the stable conformer the bond parameters were calculated by the same basis set. Results obtained at this level of theory were used for a detailed interpretation of the infrared and Raman spectra, based on the total energy distribution (TED) of the normal modes. The hyperconjugative interaction energy ($E^{(2)}$) and electron densities of donor (i) and acceptor (j) bonds were calculated using NBO analysis. The first order hyperpolarizability (β_0) was calculated. The energy gap of the molecule was found using HOMO and LUMO calculation. Atomic charges of the carbon, nitrogen and oxygen were calculated using same level of calculation.

1. Introduction

Piperidin-4-one compounds have received extensive attention in the recent years because of their diverse biological activities and form an essential part of the molecular structures of important drugs. The 2,6-Disubstituted piperidin-4-ones are regarded as an important framework and served as precursors for chiral biologically active natural alkaloids [1]. The biological activities of piperidones were found to be excellent if 2- and/or 6-positions are occupied by aryl groups [2]. In present study 3-methyl-2,6-diphenyl piperidin-4-one was synthesized by Mannich reaction (condensation) of ethylmethyl ketone, benzaldehyde and ammonium acetate. Semicarbazone derivative of 3-methyl-2,6-diphenylpiperidin-4-one were synthesized by reaction with semicarbazide hydrochloride respectively. Molecular geometry critically influences biological activity. Attention has been focused

* Corresponding author. Mobile: +91 9842483139.
E-mail addresses: drsmgac@gmail.com (S. Manivarman), sscbphysics@gmail.com (S. Subashchandrabose).

0022-2860/$ - see front matter © 2013 Elsevier B.V. All rights reserved.
http://dx.doi.org/10.1016/j.molstruc.2013.09.052

on structure–activity relationships. Apart from other organic compounds, semicarbazones and thiosemicarbazones are also known to have antiviral, antibacterial and antifungal effects in the field of medicine, pest control and are used as drugs to cure diseases [3–7]. In quantitative structure activity relationship (QSAR) studies, surface area and molecular volume are found to play an important role in the overall activity of the biologically active molecule [8]. Several semicarbazones and its derivatives have proved the efficiency and efficacy in combating various diseases [9]. Vibrational spectroscopy is a valuable tool for the elucidation of molecular structure and gives a dynamical picture of the molecule. Vibrational spectroscopy has contributed significantly to the growth of polymer chemistry, catalysis, fast reaction dynamics, etc., [10]. The philosophy of computational methods of vibrational spectroscopy changed significantly after the introduction of Scaled Quantum Mechanical calculations (SQM).

The present research work mainly focused on the synthesis of EMDPS and its FT-IR, FT-Raman vibrational spectra characterization. To support our experimental investigation the theoretical calculation such as conformational, vibrational and electronic excitation analysis were studied using B3LYP/6-311++G(d,p). For the accurate prediction of vibrational assignments the total energy distribution analysis was carried out. In addition the intra-molecular charge transfer and non-linear optical activity of the title molecule also studied.

2. Experimental details

2.1. Synthesis of (E)-1-(3-methyl-2,6-diphenylpiperidin-4-ylidene)semicarbazide[EMDPS]

Dry ammonium acetate (0.1 mol) has been dissolved in 50 ml ethanol and the solution was mixed with aromatic aldehyde (0.2 mol) and ethyl methyl ketone (0.1 mol) so as to make a homogeneous mixture. Then the mixture was heated to simmering carefully and allowed to stand at room temperature overnight. Dry ether (150 ml) was added followed by concentrated hydrochloric acid (5 ml) and the precipitated hydrochloride salt was collected and washed repeatedly with ethanol and ether (1:5) mixture. A suspension of the hydrochloride salt in acetone was treated with strong liquid ammonia solution and the free base was obtained by pouring water. The precipitated base was filtered, dried and recrystallized from absolute ethanol.

Semicarbazone derivative of 3-methyl-2,6-diphenyl-4-piperidone were synthesized by the reaction of 3-methyl-2,6-diphenylpiperidin-4-one with semicarbazide hydrochloride. A mixture of semicarbazide hydrochloride (0.01 mol) and 3-methyl-2,6-diphenyl piperidin-4-ones (0.01 mol) in ethanol (30 ml) was refluxed for 3 h with continuous stirring. Then the contents were cooled. The product was obtained by pouring it in ice water then the product was filtered, washed with water, vacuum dried and recrystallized from absolute ethanol. The yield of the compound was 80%.

2.2. FT-IR spectra and FT-Raman spectra

The FT-IR spectrum of the synthesized piperidone was measured in the 4000–400 cm^{-1} region at the spectral resolution of 4 cm^{-1} using on SHIMADZU FT-IR affinity Spectrophotometer (KBr pellet technique) made in Japan. The FT-IR spectrum was recorded in Faculty of Marine Biology, Annamalai University, parangipettai and only noteworthy absorption levels are listed. The FT-Raman spectrum of the title compound was recorded on BRUKER: RFS27 spectrometer operating at laser 100 mW in the spectral range of 4000–50 cm^{-1}. FT-Raman spectral measurements were carried out from Sophisticated Analytical Instrument Facility (SAIF), Indian Institute of Technology (IIT), Chennai.

3. Computational details

The quantum chemical calculations of EMDPS have been performed using the B3LYP/6-311++G(d,p) basis set, using the Gaussian 03 program. The entire calculations were performed at DFT levels on a Pentium 1 V/3.02 GHz personal computer using Gaussian 03W [11] program package, invoking gradient geometry optimization [11,12]. Initial geometry generated from standard geometrical parameters was minimized without any constraint in the potential energy surface at DFT level, adopting the standard 6-311++G(d,p) basis set. The optimized structural parameters were used in the vibrational frequency calculations at the DFT level to characterize all stationary points as minima. Then, vibrational averaged nuclear positions of EMDPS were used for harmonic vibrational frequency calculations resulting in IR and Raman frequencies together with intensities and Raman depolarization ratios. In this study, the DFT method (B3LYP/6-311++G(d,p)) was used for the computation of molecular structure, vibrational frequencies and energies of optimized structures. The vibrational modes were assigned on the basis of TED analysis using SQM program [13]. It should be noted that the Gaussian 03W package able to calculate the Raman activity. The Raman activities were transformed into Raman intensities using Raint program [14] by the expression:

$$I_i = 10^{-12} \times (v_0 - v_i)^4 \times \frac{1}{v_i} \times RA_i \quad (1)$$

where I_i is the Raman intensity, A_i is the Raman scattering activities, v_i is the wavenumber of the normal modes and v_0 denotes the wavenumber of the excitation laser [15]. In order to establish the stable possible conformations, the conformational space of title compound was scanned with molecular mechanic simulations. This calculation was performed with the Spartan 10 program [16]. For meeting the requirements of both accuracy and computing economy, theoretical methods and basis sets should be considered. Density functional theory (DFT) has been proved to be extremely useful in treating electronic structure of molecules. The basis set 6-311++G(d,p) was used as an effective and economical level to study. After the most stable conformer of the title compound determined, geometry optimizations of this conformer have been performed.

4. Results and discussion

4.1. Conformational stability

The chair conformer of piperidine derivatives are most stable conformer. Therefore, we neglected other conformations (boat, envelope or twist boat) for the further calculation. Moreover, it has two possible chair conformations, which differ in the axial (*A*) or equatorial (*E*) positions of the N—H group [17–19]. Piperidine molecule shows the equatorial form of N—H of chair conformer as the most stable. Piperidine derivative adopts the N—H equatorial position of the chair conformer. To find the stable conformers, a meticulous conformational analysis was carried out for the title compound. Rotating bond around the free rotation up to 360° with 10° interval, conformational space of the title compound was scanned by molecular mechanic simulations and then full geometry optimizations of these structures were performed by B3LYP/6-311++G(d,p) method. Results of geometry optimizations were indicated that the title compound may have at least 27 conformers as shown in Fig. S1 (Supporting information). Ground state energies, zero point corrected energies (Eelect. + ZPE), relative energies and dipole moments of conformers were presented in Table 1. From the calculated energies of 27 conformers the conformer one is the most stable. The optimized structure of EMDPS is shown in Fig. 1.

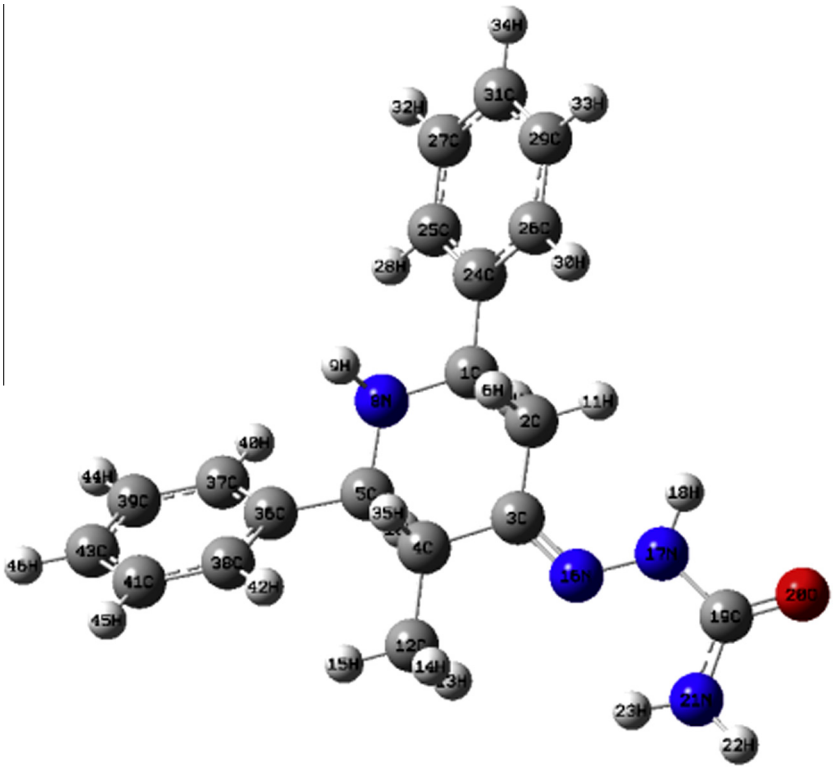

Fig. 1. The optimized molecular structure of EMDPS.

4.2. Vibrational assignments

Synthesized EMDPS is non-planar molecule and possesses C_1 point group symmetry. The molecule has 46 atoms and hence it shows 132 normal modes of vibrations, which were active in both IR absorption and Raman scattering. The fundamental vibrational wavenumbers of EMDPS was calculated by B3LYP/6-311++G(d,p). We know that the DFT potentials systematically overestimate the vibrational wavenumbers. The resulting vibrational wavenumbers, IR intensities, Raman scattering activities and experimental FT-IR and FT-Raman frequencies for the optimized structure are listed in Table 2. The discrepancies between experimental and computed wavenumbers were corrected by introducing a scaled field [20] or directly scaling the calculated wavenumbers with the proper factor

Table 1
Energetics of the conformers for EMDPS calculated at the B3LYP/6-311++G(d,p) level.

Conf.	E (Hartree)	ΔE (kcal/mol)	E_0 (Hartree)	ΔE_o (kcal/mol)	Dip. mom. (D)
Conf-1	−1031.53781508	0.0000	−1031.15218708	0.0000	4.367
Conf-2	−1031.53139008	4.0318	−1031.14587908	3.9583	4.617
Conf-3	−1031.53138992	4.0319	−1031.14586992	3.9641	4.617
Conf-4	−1031.53138998	4.0318	−1031.14586898	3.9647	4.617
Conf-5	−1031.53138993	4.0318	−1031.14586793	3.9653	4.617
Conf-6	−1031.53138989	4.0319	−1031.14586789	3.9654	4.617
Conf-7	−1031.53158503	3.9094	−1031.14564403	4.1058	4.727
Conf-8	−1031.53158501	3.9094	−1031.14564301	4.1065	4.727
Conf-9	−1031.53158496	3.9095	−1031.14564196	4.1071	4.727
Conf-10	−1031.53158506	3.9094	−1031.14564106	4.1077	4.727
Conf-11	−1031.53158495	3.9095	−1031.14563995	4.1084	4.727
Conf-12	−1031.53158503	3.9094	−1031.14563903	4.1090	4.728
Conf-13	−1031.53158507	3.9094	−1031.14563807	4.1096	4.728
Conf-14	−1031.53017498	4.7942	−1031.14451098	4.8168	4.660
Conf-15	−1031.53017563	4.7938	−1031.14451063	4.8170	4.660
Conf-16	−1031.52948845	5.2250	−1031.14366245	5.3493	4.940
Conf-17	−1031.52948845	5.2250	−1031.14366145	5.3499	4.940
Conf-18	−1031.52948843	5.2251	−1031.14366043	5.3506	4.940
Conf-19	−1031.52948838	5.2251	−1031.14365938	5.3512	4.941
Conf-20	−1031.52948841	5.2251	−1031.14365641	5.3531	4.942
Conf-21	−1031.52041123	10.9211	−1031.13418523	11.2963	4.055
Conf-22	−1031.52045381	10.8944	−1031.13328881	11.8589	5.745
Conf-23	−1031.52045382	10.8944	−1031.13328782	11.8595	5.745
Conf-24	−1031.51840879	12.1776	−1031.13154779	12.9514	5.995
Conf-25	−1031.51840872	12.1777	−1031.13154572	12.9527	5.996
Conf-26	−1031.51840883	12.1776	−1031.13154483	12.9532	5.996
Conf-27	−1031.51840885	12.1776	−1031.13154385	12.9538	5.997

E_0 – Zero point corrected energy.

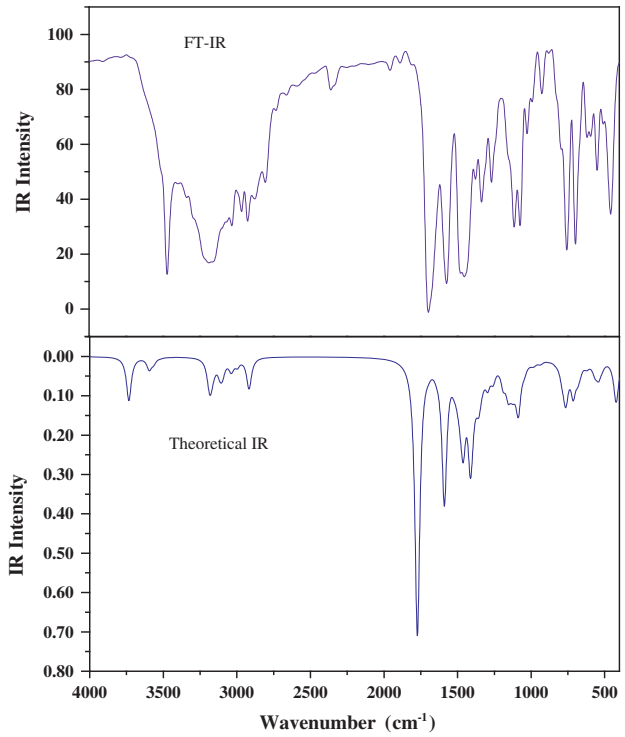

Fig. 2. The FT-IR and simulated IR spectra of EMDPS.

[21]. The FT-IR and simulated IR spectra were shown in Fig. 2. The FT-Raman and simulated Raman spectra were shown in Fig. 3. The vibrational assignments were carried out using total energy distribution calculation method equipped with scaled quantum mechanical program. To bring the theoretical values closer to experimental values, we used the scale factor: 0.9608 [22].

4.2.1. N—H vibrations

The N—H stretching vibration [17,18] appears strongly and broadly in the region 3500–3300 cm^{-1}. Erdogdu et al. assigned ν_{N-H} mode in the region 3500–3300 cm^{-1} [19]. In this study, the amino group stretching vibration was recorded as very strong band at 3468 cm^{-1} in FT-IR spectra, their corresponding computed value matches at 3455 cm^{-1} (mode no: 131) for symmetric NH_2 mode. Moreover the N—H stretching vibration appears as pure mode at the mode number 129 and 130 as calculated about 3379 and 3426 cm^{-1}, which coincides well with recorded FT-IR value of 3356 cm^{-1} (weak). The TED corresponding to this vibration is a pure mode and is exactly contributes about to 100%. The out-of-plane bending mode of $\Gamma_{HNCC(18)}$ is appeared at 756 cm^{-1} (FT-IR-strong), these vibration show a good agreement with the theoretical frequency at 760 cm^{-1} (mode no. 45). The in-plane bending mode of δ_{C-N-H} is appeared at 1403 and 1527 cm^{-1} (mode nos. 95 and 104) also find support from the literature.

4.2.2. C=O, C=N, C—N vibrations

The carbonyl C=O stretching vibration is expected to occur in the region 1680–1715 cm^{-1} [23,24]. In the present study, the C=O group stretching appeared as strong band at 1695 cm^{-1} in FT-IR spectrum and the same band was computed about 1704 cm^{-1} (mode no: 110). The both observed and calculated values are coincides well with each other. The TED analysis shows about 70% of contribution. The deviation is due to the π-electron delocalization within the molecule [25]. The intensity of the carbonyl group can increase by the conjugation or formation of hydrogen bonds. The above assignment agrees well with the value available in the literature [26].

In the present investigation ν_{N16-C3} stretching frequency observed at 1603 cm^{-1} a very strong band in FT-Raman and its theoretical frequency is about 1630 cm^{-1} (mode no: 109) and its TED value is 79%. The experimental and theoretical value for C=N band coincides well with literature [27]. The identification of C—N vibration is a very difficult task, since mixing of several bands are possible in this region. However, with the help of theoretical calculation (B3LYP), the C—N stretching vibrations are calculated. The C—N stretching vibration coupled with scissoring of N—H, is moderately to strongly active in the region 1300 cm^{-1} [28]. In the present investigation the C—N bending vibration, observed at 1403 and 1412 cm^{-1} (mode nos: 95 and 96) respectively.

4.2.3. Methyl and methylene group vibrations

Methyl groups are generally referred to as electron donating substituents in the aromatic ring system [29]. The title molecule possesses methyl (CH_3) and methylene (CH_2) groups. Methyl group symmetric stretching vibration is observed at 2922 cm^{-1} (strong bond) in FT-IR and 2925 cm^{-1} (weak band) FT-Raman are in agreement with the theoretical value of 2921 cm^{-1} (mode no: 115) its TED value is 50%. The methyl group asymmetric stretching vibration is calculated at 2994 and 2982 cm^{-1} (mode nos: 118 and 117), which are agreed well with recorded value of 2991 cm^{-1} by FT-Raman spectrum and also possesses considerable TED value. The asymmetric and symmetric CH_2 stretching vibrations are normally appear in the region 3100–2900 cm^{-1} [30]. According to the literature [31], symmetric CH_2 stretching vibrations are appeared at 2974 cm^{-1} as a weak band in FT-IR, while the scaled harmonic frequency 2973 cm^{-1} (mode no: 116) with considerable intensity is in line with experimental value and its TED value is appeared about ~87%.

In aromatic compounds the ν_{C-H}, β_{C-H} and γ_{C-H} modes are appeared in the range of 3000–3100, 1000–1300 and 750–1000 cm^{-1} respectively [32–34]. In our present study the C—H stretching vibrations appeared in the ranges of 3031–3066 cm^{-1} (mode nos: 119–128). The observed frequencies showed at 3031 cm^{-1} (FT-IR) and 3060 cm^{-1} (FT-Raman) for C—H stretching vibration. These C—H stretching vibrations are finding well supported by the TED values. The C—H in-plane bending vibrations appeared in the range 1007–1047 cm^{-1} (mode nos: 64–67) and their corresponding experimental wavenumbers 1024 cm^{-1} (FT-IR) and 1002 cm^{-1} (FT-Raman) are in consistent with computed values. The twisting, wagging and rocking vibrations appear in the region 1400–900 cm^{-1} [35]. In the present investigation, ωCH_2 and δCH_2 were calculated about 1419 and 1412 cm^{-1} (mode nos: 97 and 96) respectively. In-plane bending vibration of C—H was calculated between 1330 and 1345 cm^{-1}, whereas the observed value lies in the range of 1334 cm^{-1} in both FT-IR and FT-Raman spectra. The δ_{C-H} mode is appeared well in experimental as well as theoretical spectra.

4.3. HOMO–LUMO analysis

The frontier molecular orbitals play an important role in the electric and optical properties, and chemical reactions [26]. The analysis of the wave function indicates that the electron absorption corresponds to the transition from the ground to the first excited state and is mainly described by one electron-excitation from the highest occupied molecular orbital (HOMO) to the lowest unoccupied orbital (LUMO) [36]. The energy gap for EMDPS was calculated using B3LYP/6-311++G(d,p) level. The bioactivity and chemical activity of the molecule depends on the eigen value of HOMO, LUMO and energy gap. The LUMO as an electron acceptor represents the ability to obtain an electron; donor represents the ability to donate an electron. The energy difference between the HOMO and LUMO is about 0.20066 eV. The frontier molecular orbital of EMDPS (HOMO–LUMO) is shown in Fig. 4.

Table 2
Vibrational wave numbers obtained for EMDPS at B3LYP/6-311++G(d,p) [harmonic frequency (cm^{-1}), IR, Raman intensities (km/mol), reduced masses (amu) and force constants (mdynÅ^{-1})].

Mode no.	Calculated frequencies (cm^{-1})		Observed frequencies (cm^{-1})		Intensities		Vibrational assignments TED[d] (⩾10%)
	Unscaled	Scaled[a]	FT-IR	FT-Raman	I^{b}_{IR}	I^{c}_{Raman}	
1	23	22			0.07	100.00	$\Gamma_{C19-N17-N16-C3(10)}$
2	28	27			0.04	65.72	$\Gamma_{C25-C24-C1-N8(13)} + \Gamma_{C26-C24-C1-C2(11)} + \Gamma_{C26-C24-C1-N8(17)}$
3	37	36			0.01	71.09	$\Gamma_{C37-C36-C5-N8(16)} + \Gamma_{C38-C36-C5-C4(12)} + \Gamma_{C38-C36-C5-N8(22)}$
4	46	44			0.05	44.98	$\Gamma_{C3-C2-C1-C24(14)}$
5	49	47			0.04	44.91	$\Gamma_{C36-C5-C4-C3(10)}$
6	55	53			0.12	7.51	$\Gamma_{H18-N17-N16-C3(26)} + \Gamma_{O20-C19-N17-N16(13)} + \Gamma_{N21-C19-N17-N16(17)}$
7	73	70			0.05	8.02	$\Gamma_{C19-N17-N16-C3(10)} + \Gamma_{O20-C19-N17-N16(15)} + \Gamma_{N21-C19-N17-N16(13)}$
8	82	79			0.02	7.97	$\Gamma_{C19-N17-N16-C3(23)}$
9	101	97			0.14	8.31	$\Gamma_{C19-N17-N16-C3(14)}$
10	126	121			0.29	3.22	$\delta_{N17-N16-C3(16)} + \delta_{C19-N17-N16(16)}$
11	180	173			0.15	2.46	$\delta_{C25-C24-C1(15)} + \delta_{C37-C36-C5(10)}$
12	209	202			0.19	9.42	$\nu_{C36-C5(14)}$
13	225	217			0.49	7.18	$\nu_{C24-C1(11)}$
14	231	222		223s	0.74	0.72	$\Gamma_{H15-C12-C4-H10(12)}$
15	235	226			0.94	6.39	$\Gamma_{CCCC(19)}$
16	267	256			18.60	9.39	$\Gamma_{H22-N21-C19-N17(28)} + \Gamma_{H22-N21-C19-O20(19)} + \Gamma_{H23-N21-C19-N17(11)} + \Gamma_{H23-\ N21-C19-O20(18)}$
17	275	264			1.00	7.59	$\Gamma_{HCCC(26)}$
18	291	279			2.43	2.30	$\delta_{CCN(12)}$
19	302	290		281vs	0.06	2.45	$\delta_{C38-C36-C5(15)}$
20	307	295			1.44	0.99	$\Gamma_{N17-N16-C3-C4(10)}$
21	337	324			0.88	2.10	$\delta_{CCC(10)}$
22	415	398			0.75	0.66	$\Gamma_{N17-N16-C3-C2(10)}$
23	416	399			0.26	0.10	$\Gamma_{C31-C27-C25-C24(18)} + \Gamma_{C31-C29-C26-C24(18)}$
24	416	400			0.44	0.26	$\Gamma_{C43-C39-C37-C36(15)} + \Gamma_{C43-C41-C38-C36(15)}$
25	423	406			14.17	1.49	$\Gamma_{O20-C19-N17-H18(29)} + \Gamma_{N21-C19-N17-H18(26)}$
26	456	438			0.38	0.46	$\delta_{CCC(12)}$
27	488	469	457s		0.12	1.27	$\delta_{OCN(14)}$
28	515	494		483ms	0.56	0.70	$\delta_{CCC(10)} + \Gamma_{CCCH(12)}$
29	520	500			1.37	1.53	$\Gamma_{CCCC(12)} + \Gamma_{CCCH(10)}$
30	541	520			5.22	3.44	$\delta_{O20-C19-N17(12)} + \delta_{O20-C19-N21(14)}$
31	563	541			2.58	1.43	$\Gamma_{H22-N21-C19-N17(13)} + \Gamma_{H23-N21-C19-N17(15)}$
32	569	547	549m		1.72	0.49	$\delta_{CCC(10)}$
33	591	568			0.38	7.64	$\delta_{N21-C19-N17(12)} + \delta_{O20-C19-N21(13)} + \Gamma_{H23-N21-C19-N17(13)}$
34	616	592		591ms	0.82	2.33	$\delta_{CCC(17)}$
35	625	601			1.33	0.66	$\delta_{NCC(11)}$
36	634	609	605m		0.03	3.47	$\delta_{C39-C37-C36(11)} + \delta_{C41-C38-C36(11)} + \delta_{C43-C39-C37(13)} + \delta_{C43vC41-C38(13)}$
37	635	610			0.04	2.74	$\delta_{C27-C25-C24(11)} + \delta_{C31-C27-C25(12)} + \delta_{C31-C29-C26(13)}$
38	667	641			2.00	1.74	$\delta_{NCC(12)}$
39	683	657			4.79	5.70	$\delta_{CCC(10)}$
40	714	686			5.88	0.02	$\Gamma_{H46-C43-C39-C37(12)} + \Gamma_{H46-C43-C41-C38(12)}$
41	714	686	694vs		5.47	0.02	$\Gamma_{H34-C31-C27-C25(12)} + \Gamma_{H34-C31-C29-C26(12)}$
42	757	727			2.10	0.17	$\Gamma_{O20-C19-N17-H18(17)} + \Gamma_{N21-C19-N17-N16(13)} + \Gamma_{H22-N21-C19-O20(22)} + \Gamma_{H23-N21-C19-O20(17)}$
43	765	735			11.17	0.48	$\Gamma_{HCCC(18)} + \Gamma_{CCCH(11)}$
44	777	746			2.37	1.12	$\Gamma_{HCCC(20)} + \Gamma_{CCCH(10)}$
45	791	760	756vs		3.51	2.61	$\Gamma_{HNCC(18)} + \Gamma_{HNCH(10)}$
46	814	782			0.25	2.48	$\nu_{C4-C3(20)}$
47	834	801			0.58	0.91	$\nu_{CC(31)}$
48	858	825			0.02	0.04	$\Gamma_{HCCC(35)} + \Gamma_{CCCH(24)} + \Gamma_{HCCH(12)}$
49	861	827			0.08	0.16	$\Gamma_{HCCC(38)} + \Gamma_{HCCH(11)} + \Gamma_{CCCH(22)}$
50	880	846			0.31	12.94	$\nu_{C5-C4(16)} + \delta_{H14-C12-C4(10)}$
51	914	878		881s	0.06	1.79	$\nu_{C2-C1(11)}$
52	929	893			0.24	3.59	$\Gamma_{HCCH(10)}$
53	935	898			0.49	0.85	$\Gamma_{HCCC(25)} + \Gamma_{HCCH(21)} + \Gamma_{CCCH(15)}$

(*continued on next page*)

Table 2 (*continued*)

Mode no.	Calculated frequencies (cm^{-1})		Observed frequencies (cm^{-1})		Intensities		Vibrational assignments TED[d] (⩾10%)
	Unscaled	Scaled[a]	FT-IR	FT-Raman	I^{b}_{IR}	I^{c}_{Raman}	
54	942	905			0.61	1.76	$\nu_{CC(10)}$
55	977	939	925w		0.98	2.77	$\nu_{C19-N17(24)} + \nu_{N21-C19(42)}$
56	988	950			0.04	0.03	$\Gamma_{H44-C39-C37-H40(18)} + \Gamma_{H45-C41-C38-H42(21)}$
57	990	951			0.11	1.04	$\Gamma_{H32-C27-C25-H28(13)} + \Gamma_{H33-C29-C26-H30(19)}$
58	993	954			0.70	3.80	$\nu_{C2-C1(13)}$
59	1005	965			0.01	0.17	$\Gamma_{H44-C39-C37-H40(14)} + \Gamma_{H46-C43-C39-H44(25)} + \Gamma_{H46-C43-C41-H45(20)}$
60	1006	966			0.05	0.08	$\Gamma_{H32-C27-C25-H28(19)} + \Gamma_{H34-C31-C27-H32(24)} + \Gamma_{H34-C31-C29-H33(16)}$
61	1017	977			0.05	4.83	$\nu_{CC(24)} + \delta_{CCC(24)}$
62	1017	978			0.06	30.53	$\nu_{CC(23)} + \delta_{CCC(25)}$
63	1040	999			0.75	1.45	$\nu_{C12-C4(16)}$
64	1049	1007		1002vs	1.37	3.17	$\nu_{C43-C39(20)} + \nu_{C43-C41(18)}$
65	1049	1008			0.76	10.68	$\nu_{C31-C27(19)} + \nu_{C31-C29(19)}$
66	1086	1043	1024w		12.94	0.72	$\nu_{N8-C5(11)} + \nu_{N17-N16(12)}$
67	1089	1047			3.70	1.35	$\delta_{H22-N21-C19(14)} + \delta_{H23-N21-C19(17}$
68	1098	1055			1.00	0.31	$\nu_{C27-C25(11)} + \nu_{C29-C26(14)}$
69	1109	1065			1.24	2.11	$\nu_{N8-C5(11)}$
70	1116	1072			0.82	2.86	$\nu_{N8-C5(16)} + \nu_{C12-C4(13)}$
71	1124	1080	1078m		5.33	1.94	$\nu_{N8-C1(29)}$
72	1138	1093			3.12	8.52	$\nu_{N17-N16(13)}$
73	1156	1111	1111m		9.07	3.72	$\nu_{N8-C1(13)} + \nu_{N17-N16(24)}$
74	1181	1135			0.05	1.09	$\delta_{H46-C43-C39(17)} + \delta_{H46-C43-C41(17)}$
75	1182	1135			0.28	1.45	$\delta_{H34-C31-C27(16)} + \delta_{H34-C31-C29(16)}$
76	1190	1143			6.46	5.70	$\delta_{CCH(15)}$
77	1198	1151			0.26	0.87	$\delta_{CCH(37)} + \delta_{HCC(26)}$
78	1199	1152			0.07	1.84	$\delta_{HCC(26)} + \delta_{CCH(30)}$
79	1218	1170			0.02	4.83	$\nu_{C24-C1(13)} + \nu_{C36-C5(23)}$
80	1224	1176		1175ms	0.19	20.30	$\nu_{C24-C1(20)}$
81	1257	1208		1205ms	4.80	2.98	$\nu_{CC(21)}$
82	1269	1219			0.98	1.94	$\delta_{HCC(13)} + \Gamma_{HCCH(14)} +$
83	1295	1244			6.49	0.82	$\nu_{CC(10)}$
84	1310	1259	1265s		0.29	3.49	$\nu_{CC(19)}$
85	1325	1273			1.51	2.19	$\nu_{CC(24)}$
86	1340	1287			2.00	2.09	$\delta_{HCC(10)}$
87	1347	1294			0.16	0.25	$\nu_{C39-C37(10)}$
88	1350	1297			1.35	1.20	$\delta_{H28-C25-C24(10)}$
89	1356	1303			9.35	3.10	$\delta_{H10-C4-C12(11)}$
90	1372	1319			2.78	13.05	$\delta_{C2-C1-H6(11)}$
91	1379	1325	1334s	1334vs	0.68	5.01	$\delta_{HCC(21)} + \Gamma_{CNCH(10)}$
92	1400	1345			8.28	0.22	$\Gamma_{HCCH(12)}$
93	1413	1357			15.62	1.20	$\delta_{HCH(13)} + \delta_{HNC(15)}$
94	1415	1359			14.54	1.75	$\delta_{H13-C12-C4(12)} + \delta_{H14-C12-C4(11)} + \delta_{H13-C12-H14(14)} + \delta_{H15-C12-C4(12)} + \delta_{H13-C12-H15(14)} + \delta_{H14-C12-H15(10)}$
95	1461	1403			22.12	0.98	$\nu_{C19-N17(14)} + \delta_{H18\nu N17-N16(23)} + \delta_{H18-N17-C19(14)}$
96	1470	1412			4.31	3.38	$\delta_{H9-N8-C1(18)} + \delta_{H9-N8-C5(18)}$
97	1476	1419			2.63	0.89	$\delta_{H7-C2-H11(18)}$
98	1484	1426			1.70	0.52	$\nu_{CC(16)} + \delta_{HCC(26)} + \delta_{CCH(10)}$
99	1486	1427			3.05	0.33	$\nu_{CC(11)} + \delta_{HCC(14)}$
100	1496	1437			0.88	1.38	$\delta_{H13-C12-H14(27)} + \delta_{H13-C12-H15(24)}$
101	1503	1444			3.74	0.54	$\delta_{H14-C12-H15(33)}$
102	1524	1464			2.18	0.08	$\nu_{CC(20)} + \delta_{HCC(23)} + \delta_{CCH(22)}$
103	1524	1465	1463s		1.34	0.26	$\nu_{CC(20)} + \delta_{CCH(22)} + \delta_{HCC(22)}$
104	1590	1527			50.62	4.02	$\delta_{H23-N21-C19(21)} + \delta_{H22-N21-H23(55)}$
105	1623	1559			0.04	1.57	$\nu_{C37-C36(11)} + \nu_{C43-C39(12)} + \nu_{C43-C41(14)}$
106	1624	1560			0.26	1.98	$\nu_{C25-C24(11)} + \nu_{C26-C24(10)} + \nu_{C31-C27(12)} + \nu_{C31-C29(14)}$
107	1642	1578	1573vs		0.91	9.83	$\nu_{C39-C37(18)} + \nu_{C41-C38(17)}$
108	1643	1578			0.55	10.56	$\nu_{C27-C25(18)} + \nu_{C29-C26(17)}$
109	1697	1630		1603vs	1.18	62.15	$\nu_{N16-C3(79)}$

110	1773	1704	1695vs	100	7.81	$\nu_{O20-C19(70)}$
111	2915	2801	2804ms	5.39	2.69	$\nu_{H35-C5(99)}$
112	2919	2805		6.02	2.96	$\nu_{H6-C1(100)}$
113	2997	2879	2877w 2882ms	2.46	2.90	$\nu_{H10-C4(98)}$
114	3033	2914		1.73	3.67	$\nu_{H7-C2(87)} + \nu_{H11-C2(13)}$
115	3041	2921	2922ms 2925vs	2.72	4.76	$\nu_{H13-C12(25)} + \nu_{H14-C12(24)} + \nu_{H15-C12(50)}$
116	3095	2973	2974w	2.75	1.73	$\nu_{H7-C2(13)} + \nu_{H11-C2(87)}$
117	3104	2982		2.98	2.08	$\nu_{H13-C12(20)} + \nu_{H14-C12(31)} + \nu_{H15-C12(49)}$
118	3116	2994	2991w	3.62	2.03	$\nu_{H13-C12(55)} + \nu_{H14-C12(45)}$
119	3154	3031		0.87	1.07	$\nu_{H30-C26(76)} + \nu_{H33-C29(17)}$
120	3156	3032		0.78	0.86	$\nu_{H42-C38(62)} + \nu_{H45-C41(25)}$
121	3163	3039	3037w	0.01	2.18	$\nu_{H40-C37(10)} + \nu_{H42-C38(17)} + \nu_{H44-C39(45)} + \nu_{H46-C43(21)}$
122	3164	3040		0.02	4.63	$\nu_{H30-C26(11)} + \nu_{H32-C27(46)} + \nu_{H34-C31(28)}$
123	3173	3049		2.18	3.67	$\nu_{H40-C37(15)} + \nu_{H42-C38(14)} + \nu_{H44-C39(16)} + \nu_{H45-C41(34)} + \nu_{H46-C43(20)}$
124	3174	3050		2.39	3.53	$\nu_{H28-C25(10)} + \nu_{H32-C27(24)} + \nu_{H33-C29(37)} + \nu_{H34-C31(19)}$
125	3183	3058		3.20	1.14	$\nu_{H40-C37(50)} + \nu_{H45-C41(25)} + \nu_{H46-C43(16)}$
126	3185	3060	3060vs	2.91	2.55	$\nu_{H28-C25(39)} + \nu_{H33-C29(32)} + \nu_{H34-C31(25)}$
127	3190	3065		1.80	12.09	$\nu_{H40-C37(23)} + \nu_{H44-C39(26)} + \nu_{H45-C41(16)} + \nu_{H46-C43(33)}$
128	3191	3066		1.36	11.43	$\nu_{H28-C25(43)} + \nu_{H32-C27(23)} + \nu_{H33-C29(11)} + \nu_{H34-C31(21)}$
129	3517	3379	3356w	0.17	2.36	$\nu_{H9-N8(100)}$
130	3566	3426		1.86	3.30	$\nu_{H18-N17(100)}$
131	3596	3455	3468vs	4.21	4.20	$\nu_{H22-N21(36)} + \nu_{H23-N21(64)}$
132	3734	3587		15.84	1.18	$\nu_{H22-N21(64)} + \nu_{H23-N21(36)}$

ν: Stretching, δ: in-plane-bending, Γ: out-of-plane bending, vw: very weak, w: weak, m: medium, s: strong, vs: very strong.

[a] Scaling factor: 0.9608.

[b] Relative IR absorption intensities normalized with highest peak absorption equal to 100.

[c] Relative Raman intensities calculated by equation and normalized to 100.

[d] Total energy distribution calculated at B3LYP/6-311++G(d,p) level.

HOMO energy = −0.23651 eV
LUMO energy = −0.03585 eV
Energy gap = 0.20066 eV

The smaller band gap energy increases the stability of the molecule. The charge distribution of the molecule has calculated using B3LYP/6-311++G(d,p) level. This calculation depicts the charges of the every atom in molecule. Distribution of positive and negative charges is the cause, to increase or decrease of bond length. The atomic charges of carbon, nitrogen and oxygen are listed in Table 3, in which nitrogen atom possesses maximum negative charge about −0.013 a.u. The HOMO part is located over the N_{17}—C_{19}, N_{16}—C_3 orbital, is mainly due to the lone pair of electron. Some of the carbon atoms only have positive charge about C_4 (0.345), C_{19} (0.236), C_{24} (0.657), C_{25} (0.010 a.u.), C_{36} (0.638) and C_{38} (0.144). This clearly explains that the LUMO exist in those areas. The graphical representation of Mulliken atomic charge of each atom is shown in Fig. 5.

4.4. Prediction of hyperpolarizability

The first hyperpolarizabilities (β_0, α and μ) of EMDPS is calculated using B3LYP/6-311++G(d,p) level of theory, based on the finite-field approach. In the presence of an applied electric field, the energy of a system is a function of the electric field. First hyperpolarizability is a third rank tensor that can be described by a $3 \times 3 \times 3$ matrix. The 27 components of the 3D matrix can be reduced to 10 components due to Kleinman symmetry [37]. It can be given in the lower tetrahedral format. It is obvious that the lower part of the $3 \times 3 \times 3$ matrixes is a tetrahedral. The components of β are defined as the coefficients in the Taylor series expansion of the energy in the external electric field. When the external electric field is weak and homogeneous, this expansion becomes:

$$E = E^0 - \mu_\alpha F_\alpha - 1/2\alpha_{\alpha\beta}F_\alpha F_\beta - 1/6\beta_{\alpha\beta\gamma}F_\alpha F_\beta F_\gamma \quad (2)$$

where E^0 is the energy of the unperturbed molecules, F_α is the field at the origin, and μ_α, $\alpha_{\alpha\beta}$, $\beta_{\alpha\beta\gamma}$ is the components of the dipole moment, polarizability and the first hyperpolarizabilities, respectively. The total static dipole moment μ, the mean polarizability α_0, the anisotropy of polarizability $\Delta\alpha$ and the mean first hyperpolarizability β_0, using the x, y, z components are defined as

$$\mu = \left(\mu_x^2 + \mu_y^2 + \mu_z^2\right)^{1/2} \quad (3)$$

$$\alpha_0 = \frac{\alpha_{xx} + \alpha_{yy} + \alpha_{zz}}{3} \quad (4)$$

$$\Delta\alpha = 2^{-1/2}[(\alpha_{xx} - \alpha_{yy})^2 + (\alpha_{yy} - \alpha_{zz})^2 + (\alpha_{zz} - \alpha_{xx})^2 + 6(\alpha_{xy}^2 + \alpha_{yz}^2 + \alpha_{xz}^2)]^{1/2} \quad (5)$$

$$\beta_0 = \left(\beta_x^2 + \beta_y^2 + \beta_z^2\right)^{1/2} \quad (6)$$

Many organic molecules, containing conjugated π electrons are characterized by large values of molecular first hyper polarizabilities, were analyzed by means of vibrational spectroscopy [38–41]. The intra-molecular charge transfer from the donor to acceptor group through a single–double bond conjugated path can induce large variations of both the molecular dipole moment and the molecular polarizability, making IR and Raman activity strong at the same time [42].

The present study reveals that the π–π interaction can make larger intra-molecular interaction and hence the polarizability of the molecule increases. It is evident from Table 4, the molecular dipole moment (μ), molecular polarizability and hyperpolarizability

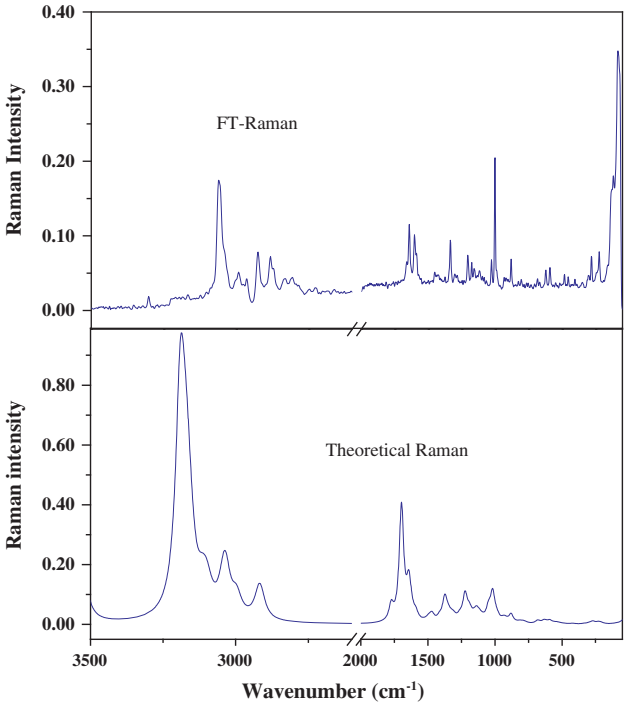

Fig. 3. The combined FT-Raman and simulated Raman spectra of EMDPS.

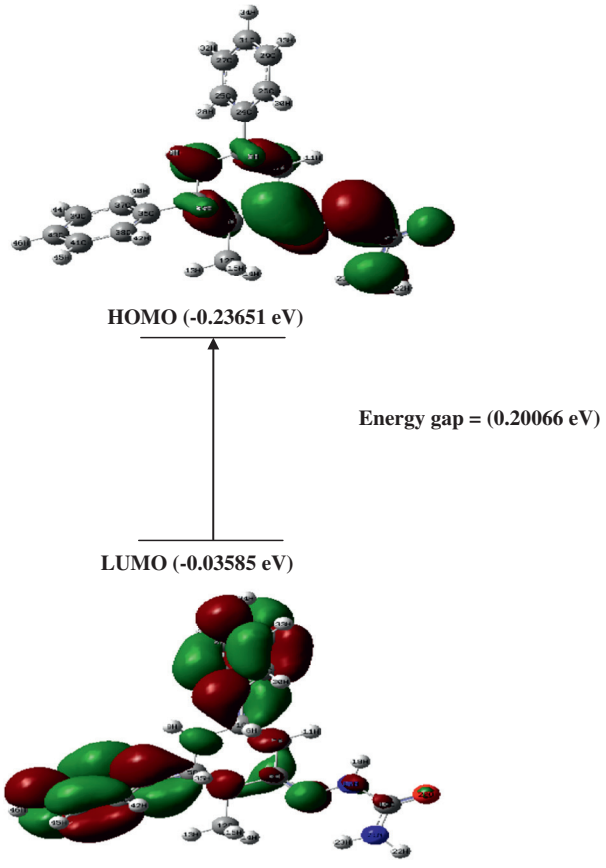

Fig. 4. The frontier molecular orbital's of EMDPS.

Table 3
Atomic charge of EMDPS.

Atoms charges (a.u.)		Atoms charges (a.u.)	
C_1	−0.034	C_{24}	0.657
C_2	−0.390	C_{25}	0.010
C_3	−0.481	C_{26}	−0.129
C_4	0.345	C_{27}	−0.041
C_5	−0.100	C_{29}	−0.231
N_8	0.368	C_{31}	−0.145
C_{12}	−0.239	C_{36}	0.638
N_{16}	0.270	C_{37}	−0.140
N_{17}	−0.013	C_{38}	0.144
C_{19}	0.236	C_{39}	−0.142
O_{20}	−0.339	C_{41}	−0.178
N_{21}	0.114	C_{43}	−0.177

are calculated about 1.8243 Debye, 0.6396 and 3.689 × 10^{-30} esu, respectively. The β_0 value of the title compound is ~9.8 times greater than that of urea.

4.5. NBO analysis

The hyperconjugation may be given as stabilizing effect that arises from an overlap between an occupied orbital with another neighboring electron deficient orbital when these orbitals are properly orientation. This non-covalent bonding–antibonding interaction can be quantitatively described in terms of the NBO analysis, which is expressed by means of the second-order perturbation interaction energy ($E^{(2)}$) [43–46]. This energy represents the estimation of the off-diagonal NBO Fock matrix elements. It can be deduced from the second-order perturbation approach [47]

$$E^{(2)} = \Delta E_{ij} = q_i \frac{F(i,j)^2}{\varepsilon_j - \varepsilon_i} \tag{7}$$

where q_i is the donor orbital occupancy, ε_i and ε_j are diagonal elements (orbital energies) and $F(i,j)$ is off diagonal NBO Fock matrix elements. In this present study the amount of energy transfer from π bond orbital to anti bond (π^*) orbital, the stabilization energy $E^{(2)}$ associated with hyperconjugative interaction, LPO(2) → N17—C19, and C19—N21 are obtained as 102.36 and 96.55 kJ/mol, respectively. The bond C29—C31 with electron density 1.6641e, stabilize the energy of 83.72 and 84.39 kJ/mol to its acceptor anti bonding orbitals of C24—C26 and C25—C27, respectively. These interactions are observed as an increase in electron density (ED) in C—C antibonding orbital that weaken their bonds [48]. This investigation clearly demonstrates that the occupancy value of bonding orbitals make sure the hyperconjugative interaction with maximum stabilization between filled and unfilled subsystem of the molecule.

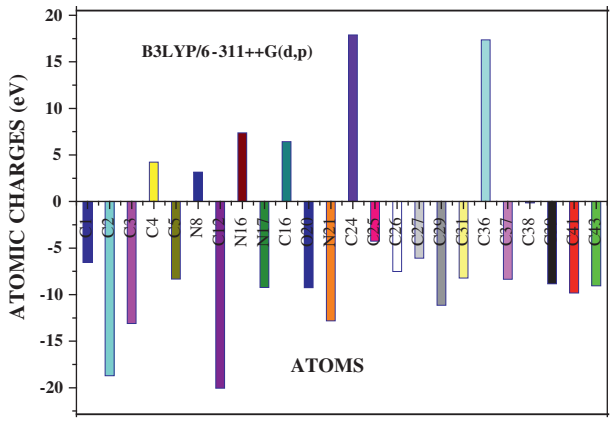

Fig. 5. The atomic charge plot of EMDPS.

Table 4
Prediction of hyperpolarizability of EMDPS.

Parameters	Hyperpolarizability
β_{xxx}	−58.47
β_{xxy}	20.68
β_{xyy}	105.04
β_{yyy}	152.52
β_{xxz}	−81.07
β_{xyz}	−70.69
β_{yyz}	−120.67
β_{xzz}	67.70
β_{yzz}	81.35
β_{zzz}	−121.50
β_0	3.689×10^{-30} esu
Parameters	Polarizability
α_{xx}	286.41
α_{xy}	19.52
α_{yy}	275.17
α_{xz}	11.40
α_{yz}	−53.88
α_{zz}	234.25
α	0.6396×10^{-30} esu
Parameters	Dipole moment
μ_x	0.3794
μ_y	1.3117
μ_z	−1.2098
μ	1.8243 Debye

Standard value for urea $\mu = 1.3732$ Debye, $\beta_0 = 0.3728 \times 10^{-30}$ esu.

From the NBO analysis, the lower the ED of donor with larger the ED of acceptor have maximum delocalization and become strong interaction. The higher the ED value with lower $E^{(2)}$ energy which becomes lesser interaction and hence it shifts the vibrational frequencies from the actual frequency range. It is evident that the C1—N8 (1.980e) and C5—N8 (1.979e) bond bending vibration (B3LYP-1412 cm^{-1}; mode no. 96). The C3—N16 (1.988e) bond stretching vibration appears at 1603 cm^{-1} (mode no. 109). The C19—N21 (1.991e) and N17—C19 (1.988e) bond bending vibrations (B3LYP-1527 and 1403 cm^{-1}; mode nos. 104 and 95) these vibrations are higher from the normal C—N bond stretching (1300 cm^{-1}) [27]. This may be due to the hyperconjugative interaction between C—N donor bonds to C—C acceptor bands.

The intra-molecular hyperconjugative interactions is due to the overlap between π (C—C) and π*(C—C) orbitals, which results intra-molecular charge transfer appeared in the molecular system [42]. It is evident from our calculation, the $E^{(2)}$ energy of πC29—C31 versus π*C24—C26 is about 83.72 kJ/mol, and their electron densities are 1.664 and 0.348e respectively. Similarly, the π–π* interaction of C25—C27 → C29—C31, C29—C31 → C24—C26, C36—C38 → C37—C39, C37—C39 → C41—C43, C41—C43→C36—C38 bonds revealed the maximum hyperconjugative interaction energy $E^{(2)}$ in both the phenyl rings are having smaller electron densities than σ bonds. The above interactions are observed as an increase in electron density (ED) in C—C anti bonding orbital that weakens the respective donor bonds. The movement of π electron from donor (*i*) to acceptor (*j*) can make the molecule highly active. It is evident from the Table 5, the n–π* interactions of N17 → C3—N16, N17 → C19—O20 and N21 → C19—O20 reveal the maximum $E^{(2)}$ energy 123.26, 149.01 and 162.01 kJ/mol respectively. The $E^{(2)}$ values and types of the transition are shown in Table 5.

5. Conclusions

In the present work, we have performed both experimental and theoretical vibrational analysis of EMDPS. The observed FT-IR and

Table 5
Second order perturbation theory of fock matrix in NBO basis for EMDPS using B3LYP/6-311++G(d,p).

Type	Donor (*i*)	ED/e	Acceptor (*j*)	ED (e)	$E^{(2)}$ (kJ/mol)[a]	$E_j - E_i$ (a.u.)[b]	$F(i,j)$ (a.u.)[c]
σ–σ*	C1—N8	1.98087	C5—C36	0.02817	6.3118	1.13	0.037
σ–σ*	C3—N16	1.98809	C2—C3	0.03893	6.6044	1.33	0.041
			N17—C19	0.08036	7.524	1.34	0.045
π–σ*	C3—N16	1.95557	C2—H7	0.01673	9.9902	0.73	0.038
			C4—C5	0.03884	8.36	0.69	0.033
			C4—H10	0.02766	10.659	0.73	0.039
σ–σ*	C5—N8	1.97942	C1—C24	0.02851	6.8134	1.13	0.038
σ–π*			C36—C38	0.34543	5.225	0.75	0.03
σ–σ*	N8—H9	1.97976	C1—C2	0.0294	11.7876	0.96	0.046
			C4—C5	0.03884	10.3664	0.96	0.044
σ–σ*	N17—C19	1.98844	C3—N16	0.1862	9.6976	1.43	0.052
			N21—H22	0.00582	7.1478	1.24	0.041
σ–σ*	C19—N21	1.99195	N17—H18	0.03476	7.9002	1.21	0.043
π–σ*	C24—C26	1.66122	C1—C2	0.0294	13.5014	0.61	0.043
π–π*			C25—C27	0.01556	82.2206	0.28	0.067
π–π*	C25—C27	1.66387	C24—C26	0.34892	89.2012	0.28	0.07
			C29—C31	0.32885	84.4778	0.28	0.067
π–π*	C29—C31	1.66413	C24—C26	0.34892	83.7254	0.29	0.068
			C25—C27	0.3213	84.3942	0.28	0.068
π–σ*	C36—C38	1.66194	C4—C5	0.03884	13.376	0.61	0.043
π–π*			C37—C39	0.31903	82.2206	0.28	0.067
			C41—C43	0.32817	85.8572	0.28	0.068
σ–σ*	C37—C39	1.9783	C5—C36	0.02817	15.3824	1.11	0.057
π–π*	C37—C39	1.66541	C36—C38	0.02298	88.616	0.29	0.07
			C41—C43	0.32817	84.7704	0.28	0.068
n–π*	LP (1) N 17	1.71453	C3—N16	0.1862	123.2682	0.29	0.085
n–σ*			C19—O20	0.05277	7.5658	0.83	0.037
n–π*			C19—O20	0.33716	149.017	0.35	0.102
n–σ*	LP (2) O 20	1.84904	N17—C19	0.08036	102.3682	0.66	0.115
			C19—N21	0.06631	96.558	0.7	0.116
n–σ*	LP (1) N 21	1.78573	C19—O20	0.05277	10.3664	0.82	0.042
			C19—O20	0.33716	162.0168	0.35	0.108

[a] $E^{(2)}$ means energy of hyper conjugative interaction (stabilization energy).
[b] $E(j) - E(i)$ energy difference between donor and acceptor *i* and *j* NBO orbitals.
[c] $F(i,j)$ is the Fock matrix element between *i* and *j* NBO orbitals.

FT-Raman spectral values were agreed well with the calculated wavenumbers. All possible conformers are calculated by rotation of torsion angle. All the vibrational bands which are observed in the FT-IR and FT-Raman spectra of the title compound are completely assigned for the first time with the help of TED. The conformer one is more stable and hence the calculated wavenumbers were correlated well with the experimental values. The NBO analysis reveals that the occurrence of hyperconjugative interaction and the charge delocalization around the bonds. The HOMO–LUMO indicates that the stability and reactivity of the title compound proposed by means of energy band gap (0.20066 eV). The thermodynamic data provide helpful information for the further study on the title compound. The atomic charges of the present molecule has been calculated and also plotted.

Appendix A. Supplementary material

Supplementary data associated with this article can be found, in the online version, at http://dx.doi.org/10.1016/j.molstruc.2013.09.052.

References

[1] A. Numata, T. Ibuka, A. Brossi, In the Alkaloids, vol. 31, Academic Press, New York, 1987. p. 193.
[2] M.W. Edwards, J.W. Daly, C.W. Myers, J. Nat. Prod. 51 (1988) 1188–1197.
[3] P.D. Robinson, C.Y. Meyers, V.M. Kolb, Acta Crystallogr. C 50 (1994) 732–734.
[4] S.K. Sengupta, O.P. Pandey, G.P. Rao, D. Alpana, S. Priyanka, Phosphorus, Sulfur Silicon Relat. Elem. 178 (2003) 839–849.
[5] J.F. Borel, S. Lazary, H. Stahelin, Inflammation Res. 4 (1974) 357–363.
[6] B. Aida, M. Tados, El-Batouti, Anti-Corros. Methods Mater. 51 (2004) 406–413.
[7] T. Hemalatha, P.K.M. Imran, A. Gnanamani, S. Nagarajan, Nitric Oxide (Chem. Biol.) 19 (2008) 303–311.
[8] R. Galeazzi, C. Marucchini, M. Orena, C. Zadrab, J. Mol. Struct. (THEOCHEM) 640 (2003) 191–200.
[9] N. Fahmi, R.V. Singh, J. Indian Chem. Soc. 73 (1996) 257–259.
[10] D.N. Sathyanarayana, Vibrational Spectroscopy—Theory and Applications, second ed., New Age International (P) Limited Publishers, New Delhi, 2004.
[11] M.J. Frisch, G.W. Trucks, H.B. Schlegel, G.E. Scuseria, M.A. Robb, J.R. Cheeseman, J.A. Montgomery Jr., T. Vreven, K.N. Kudin, J.C. Burant, J.M. Millam, S.S. Iyengar, J. Tomasi, V. Barone, B. Mennucci, M. Cossi, G. Scalmani, N. Rega, G.A. Petersson, H. Nakatsuji, M. Hada, M. Ehara, K. Toyota, R. Fukuda, J. Hasegawa, M. Ishida, T. Nakajima, Y. Honda, O. Kitao, H. Nakai, M. Klene, X. Li, J.E. Knox, H.P. Hratchian, J.B. Cross, C. Adamo, J. Jaramillo, R. Gomperts, R.E. Stratmann, O. Yazyev, A.J. Austin, R. Cammi, C. Pomelli, J.W. Ochterski, P.Y. Ayala, K. Morokuma, G.A. Voth, P. Salvador, J.J. Dannenberg, V.G. Zakrzewski, S. Dapprich, A.D. Daniels, M.C. Strain, O. Farkas, D.K. Malick, A.D. Rabuck, K. Raghavachari, J.B. Foresman, J.V. Ortiz, Q. Cui, A.G. Baboul, S. Clifford, J. Cioslowski, B.B. Stefanov, G. Liu, A. Liashenko, P. Piskorz, I. Komaromi, R.L. Martin, D.J. Fox, T. Keith, M.A. Al-Laham, C.Y. Peng, A. Nanayakkara, M. Challacombe, P.M.W. Gill, B. Johnson, W. Chen, M.W. Wong, C. Gonzalez, J.A. Pople, Gaussian 03, Revision C.02, Gaussian Inc., Wallingford, CT, 2004.
[12] H.B. Schlegel, J. Comput. Chem. 3 (1982) 214–218.
[13] G. Rauhut, P. Pulay, J. Phys. Chem. 99 (1995) 3093.
[14] D. Michalska, Raint Program, Wroclaw University of Technology, 2003.
[15] D. Michalska, R. Wysokinski, Chem. Phys. Lett. 403 (2005) 211–217.
[16] Spartan 10, Wavefunction Inc., Irvine, CA 92612, USA, 2010.
[17] M.T. Gulluoglu, Y. Erdogdu, S. Yurdakul, J. Mol. Struct. 834 (2007) 540–547.
[18] Y. Erdogdu, M.T. Gulluoglu, S. Yurdakul, J. Mol. Struct. 889 (2008) 361–370.
[19] Y. Erdogdu, M.T. Gulluoglu, Spectrochim. Acta 74A (2009) 162–167.
[20] P. Pulay, G. Fogarasi, G. Pongor, J.E. Boggs, V. Vargha, J. Am. Chem. Soc. 10 (1983) 7037.
[21] A.P. Scott, L. Random, J. Phys. Chem. 100 (1996) 16502.
[22] M.A. Palafox, Int. J. Quant. Chem. 77 (2000) 661–684.
[23] N.P.G. Roeges, A Guide to the Complete Interpretation of Infrared Spectra of Organic Structure, Wiley, New York, 1994.
[24] M. Barthes, G. De Nunzio, M. Ribet, Synth. Met. 76 (1996) 337–340.
[25] C.Y. Panicker, H.T. Varghese, D. Philip, H.I.S. Nogueira, K. Kastkova, Spectrochim. Acta 67 (2007) 1313–1320.
[26] I. Fleming, Frontier Orbitals and Organic Chemical Reactions, Wiley, London, 1976.
[27] Natesh Rameshkumar, Raju Ilavarasan, Biol. Pharm. Bull. 26 (2) (2003) 188–193.
[28] N.P.G. Roeges, A Guide to the Complete Interpretation of Infrared Spectra of Organic Structures, Wiley, New York, 1994.
[29] W.B. Tzeng, K. Narayanan, J.L. Lin, C.C. Tung, Spectrochim. Acta 55A (1998) 153–162.
[30] I.H. Joe, G. Aruldhas, S.A. Kumar, P. Ramasamy, Cryst. Res. Technol. 29 (1994) 685.
[31] R.R. Sampathkumar, R. Sabesan, S. Krishnan, J. Mol. Liquids 126 (2006) 130–134.
[32] D. Lin-Vein, N.B. Colthup, W.G. Fateley, J.G. Grasselli, The Hand Book of Infrared and Raman Characteristic Frequencies of Organic Molecules, Academic Press, San Diego, 1991.
[33] M. Silverstein, G. ClytonBasseler, C. Morill, Spectrometric Identification of Organic Compounds, Wiley, New York, 1981.
[34] N. Sundaraganesan, S. Ilakiyamani, B.D. Joushua, Spectrochim. Acta 67A (2007) 287–297.
[35] J.G. Mesu, T. Visser, F. Soulimani, B.M. Weckhuysen, Vib. Spectrosc. 39 (2005) 114–125.
[36] I. Sidir, Y.G. Sidir, M. Kumalar, E. Tasal, J. Mol. Struct. 964 (2010) 134.
[37] N.B. Colthup, L.H. Daly, S.E. Wiberly, Introduction to Infrared and Raman Spectroscopy, Academic Press, New York, 1990.
[38] C. Castiglioni, M. Del zoppo, P. Zuliani, G. Zerbi, Synth. Met. 74 (1995) 171–177.
[39] P. Zuliani, M. Del zoppo, C. Castiglioni, G. Zerbi, S.R. Marder, J.W. Perry, Chem. Phys. 103 (1995) 9935.
[40] M. Del zoppo, C. Castiglioni, G. Zerbi, Non-Linear Opt. 9 (1995) 73.
[41] M. Del zoppo, C. Castiglioni, P. Zuliani, A. Razelli, G. Zerbi, M. Blanchard-Desce, J. Appl. Polym Sci. 70 (1998) 73.
[42] C. Ravikumar, I. Huber Joe, V.S. Jayakumar, Chem. Phys. Lett. 460 (2008) 552–558.
[43] A.E. Reed, F. Weinhold, J. Chem. Phys. 83 (1985) 1736.
[44] A.E. Reed, R.B. Weinstock, F. Weinhold, J. Chem. Phys. 83 (1985) 735.
[45] A.E. Reed, F. Weinhold, J. Chem. Phys. 78 (1983) 4066.
[46] J.P. Foster, F. Wienhold, J. Am. Chem. Soc. 102 (1980) 7211–7218.
[47] J. Chocholousova, V. Vladimir Spirko, P. Hobza, Phys. Chem. Chem. Phys. 6 (2004) 37–41.
[48] B. Smith, Infrared Spectral Interpretation: A Systemic Approach, CRC, Washington, DC, 1999.